Theoretical and experimental binding energies for the $d^7s^2\,{}^4F$ levels in Ru^-, including calculated hyperfine structure and $M1$ decay rates

Peggy L. Norquist and Donald R. Beck
Physics Department, Michigan Technological University, Houghton, Michigan 49931

René C. Bilodeau, Michael Scheer, Raphaël A. Srawley, and Harold K. Haugen*
Department of Physics and Astronomy, McMaster University, Hamilton, Ontario, Canada L8S 4M1
(Received 5 August 1998)

Relativistic configuration interaction (RCI) calculations predict that the $4d^75s^22J=9$, 7, 5 and 3 ${}^4F$ levels of Ru^- are all bound with binding energies 1.076, 0.905, 0.795, and 0.725 eV, respectively. Using laser photodetachment threshold spectroscopy, the binding energies of the $2J=9$ and $2J=7$ levels are measured to be 1.04638(25) and 0.8653(10) eV, respectively, in good agreement with the calculated values. Hyperfine structure constants for all levels and magnetic dipole decay rates have also been calculated, and a systematic study of the important role of quadruple excitations is presented. [S1050-2947(99)04503-5]

PACS number(s): 32.10.Hq, 32.10.Fn, 32.70.Cs, 32.80.Gc

I. INTRODUCTION

For different reasons, negative ions pose substantial challenges to the experimental and theoretical communities. For the theorist, electron correlation effects can be the dominant contribution to the electron affinity (EA, of the neutral atom), and for the medium to high Z species, of interest here, relativistic effects need to be included from the outset in any calculation. Experimentally, negative ions are often difficult to form in high concentrations, and they can be quite fragile, easily detaching electrons [1]. As for transition-metal negative ions, aside from Tc^- and Re^-, the least studied [2] species are Ru^- and Os^-. Previously, only semiempirical (by extrapolation) results existed [3], which predict a bound ground state $d^7s^2\,{}^4F$ with binding energies ~ 1.1 eV. In this work, we report relativistic configuration interaction (RCI) results for Ru^-. We are currently obtaining theoretical and experimental results for Os^-.

In addition, the results of laser photodetachment threshold (LPT) spectroscopy experiments on the ${}^4F_{9/2}$ and ${}^4F_{7/2}$ levels of Ru^- are reported. As with most transition-metal negative ions, Ru^- detaches into a p-wave continuum. A p-wave threshold can be very challenging to measure with high-precision infrared LPT spectroscopy, because of the very gradual onset of the threshold. The current work is based on the method recently demonstrated by the authors on bound states of a number of other transition-metal negative ions [4,5].

Recent relativistic correlated fully *ab initio* treatments of medium to high Z negative ions include at least four different, though related, approaches, which are (references given are only illustrative and not comprehensive) multiconfigurational Dirac-Fock [6], RCI, relativistic many-body perturbation theory [7], and relativistic coupled cluster theory [8]. Currently, a strength of the first two methods lies in their general applicability, whereas a strength of the last two lies in their achieved accuracy for ''simple'' systems. One may also note the closely related work of the ''Russian group'' [9] which is competitive, though not always fully *ab initio*.

II. THEORETICAL METHODOLOGY

We begin by solving the Dirac-Fock equations for the dominant configuration using Desclaux's program [10] and a Dirac-Coulomb Hamiltonian. This provides a reference function (DF), which is then improved systematically, by using perturbation theory to provide a form for the correlated part of the wave function. Initially, we make single and double excitations from the DF function's outermost subshells (e.g., $4d$ and $5s$ for Ru). Subshells not present in the DF function are called ''virtual,'' and their radial functions are represented by relativistic screened hydrogenic functions, with effective charge Z^*. The unknowns, Z^*, and the correlation functions' coefficients are determined by application of the variational principle, which leads to the relativistic configuration interaction (RCI) matrix [11]. In practice, electronlike solutions are assured by constraining the virtual's radial functions to have an $\langle r\rangle$ similar to the DF radial function they are replacing; we also find requiring $n=l+1$ to yield the best convergence.

During computation, several decisions must be made. (i) At what symmetry (l) are the virtuals cut off? In practice, $l=4$ is usually sufficient. (ii) How many radial functions are needed per l? Usually 2 for each l, per originating shell, is sufficient. (iii) How much of the core is excited (opened)? For the most accurate results presented here (atom and $2J=9$ ion), it appears opening the outermost closed p shell is adequate. (iv) Do we need to go beyond a first-order (singles and doubles) ''form,'' and if so what must be included? Briefly, the answer is yes, as can be determined by monitoring the largest valence energy contributions (e.g., $5s^2\rightarrow p^2$) as the core is opened. These decline as the core is opened. We interpret this as partly being due to the pulling away of e.g., $5s^2$ from $5p^2$, due to the greater amount of correlation

*Also with the Department of Engineering Physics, the Brockhouse Institute for Materials Research, and the Center for Electrophotonic Materials and Devices.

introduced in $5s^2$ as the core is opened. We partly correct this [12] by introducing the equivalent correlation into $5p^2$; such configurations are frequently triple or quadruple excitations with respect to DF, so that we are beginning to construct a second-order wave function. The remainder of the correction arises from other quadruple excitations formed from products of the largest pair excitations. These partially cancel the pair-pair interactions which decrease the correlation energy.

Due to the presence of open-shell d electrons, most correlation configurations can have many parents (a few thousand), which are constructed from many determinants ($\leqslant 14\,000$ here). Left in this form, one could be dealing with an RCI matrix of one hundred thousand parents, involving matrix elements which are constructed from (double) sums of tens of thousands of determinants. However, within the first order (in form) correlated wave function, one can reduce the number of correlation parents greatly, by realizing that their interaction with the DF (zeroth-order) function can be expressed in terms of a small number of radial integrals. To use this, we rotate the original set of parents, for each nonrelativistic manifold (group of relativistic configurations reducing to the same configuration in the nonrelativistic limit), to maximize the number of zeros. Rotated parents having zero interaction with the DF reference function are discarded. This process is called REDUCE and has been automated [13]. Calculations for Zr I [14] using REDUCE introduced errors in the total energy of 10–20 meV as compared to a calculation when REDUCE was not used.

In carrying out this work, and especially that for the homologous Os-Os^- case [15], it was found that rather large errors in the EA existed (above 100 meV for Os-Os^-), when obtained in the conventional way. Results presented here will demonstrate that this is mainly due to the absence of a few important quadruple excitations in the negative ions, and that which excitations these are can be predicted *a priori*, based on energy analysis tables such as Table I of this work. Such excitations are needed to help correct the well known size inconsistency in the CI process.

Basically, these important quadruple effects arise from products of the most important pair contributions, viz. products of $5s^2 \rightarrow p^2, 4d5s \rightarrow p^2 + sd + pf$. But, treatment of these excitations requires substantial revision of our existing algorithm [13], for two reasons: (i) the number of determinants in the final rotated functions greatly exceeds the existing limit of 5000 (at least 25 000 will be needed); (ii) each quadruple excitation will have multiple references (pair excitations), and some of these will be REDUCE vectors themselves. This is a ''new'' type of reference function, as well as being more complicated, and new programming must be done to accommodate them. It is of course desirable to keep the number of reference functions to a minimum, because the number of final (rotated) quadruple vectors kept is directly proportional to this number. As an illustration, the $4d^5vp^2vf^2 2J=9$ rotated manifold has 33 vectors formed from 13 935 determinants. Prior to rotation, there were 4598 vectors, so we have achieved a reduction of a factor of 139. It is important to understand that the more complicated the atomic state (greater number of open d/f subshell electrons), the *larger* the reduction.

After diagonalization, the size of the RCI matrix may be further reduced (allowing for additional configurations) by removing ''small'' parents (''scrubbing''). For single and double excitations, this may be done on an energy basis [16]. For triple and quadruple excitations, we use a coefficient test. Currently energy and coefficient thresholds are 0.04 meV and 0.0004, and they result in removal of about 50% of the parents, with only a few meV loss in total energy. For $Ru^- 2J=9$, the fully scrubbed REDUCE'd matrix is of order 5619.

A final computational advantage lies in the fact that all states (atom and ion) involve the d^7 electrons ''pretty much'' coupled to a ^4F. We would expect that, to a considerable degree, correlation associated with just these electrons will be much the same for all states, and so can be ignored. This strategy should be most effective for the ion states, as we have seen for Sn^- [12] where the terms, but not the configurations, do change. We make use of this by doing less extensive calculations (p shell remaining closed; limited triple and quadruple excitations) for $2J=7$, 5, and 3 and computing their energy differences with the ''cruder'' (p shell remaining closed, etc.) $2J=9$ state. In this process, it is essential that all states be treated at the same correlation level (equivalent basis sets).

Once the RCI wave functions are generated, both hyperfine structure (HFS) constants (dipole and quadrupole) and magnetic dipole ($M1$) decay rates are obtained. Expressions for HFS matrix elements have been given elsewhere [14] and are based on earlier work of Lindgren and Rosen [17]. Expressions for $M1$ transition rates have been given in Ref. [12]; they are based on the work of Grant [18]. It should be noted that since the RCI wave functions are obtained independently of one another, their basis sets are not orthonormal. In calculating the $M1$ decay rates, nonorthonormality effects are fully accounted for [19] following the work of King *et al.* [20].

The Breit contribution has been treated only at the average [10] energy DF level. Nonaverage magnetic effects are below 0.05 meV. Breit contributions to EAs are small, ~ 1 meV, so that a more thorough treatment is unnecessary.

III. EXPERIMENTAL METHOD

A schematic diagram of the experimental apparatus is shown in Fig. 1. A more detailed description of the experimental apparatus can be found elsewhere [5]. A 13 keV beam of negative ions is produced with a cesium sputter source and mass analyzed with a 30° bending magnet, set to produce a 4.4 kG magnetic field. The beam then passes through a differential pumping tube and enters an ultrahigh-vacuum (UHV) chamber where pressures of $\sim 10^{-8}$ mbar are maintained. A pair of electrostatic deflection plates serves to charge-state analyze and direct the beam to cross a pulsed laser beam at 90°. The photodetached neutral atoms are detected with a discrete-dynode electron multiplier while the residual negative ions are deflected by a second set of electrostatic plates into a Faraday cup, where currents of ≈ 2.5 nA of Ru^- are observed. A boxcar averager with an ≈ 125 ns gate, triggered via the laser pulse, integrates the signal from the detector. The integrated signal is collected by a personal computer and recorded for subsequent analyses.

The 1000–1375 nm tunable infrared laser light required in

TABLE I. Energy contributions in eV to $Ru^- 4d^7 5s^2 2J=9$ and Ru $4d^7 5s 2J=10$. (Assigned according to ''first-order'' analysis [16]. Triple and quadruple excitations given as ''0.'')

Excitation	$Ru^- 2J=9$ No quads	$Ru^- 2J=9$ With quads	Ru $2J=10$
DF	0.3167	0.3167	0
$5s^2 \rightarrow s^2$	−0.0522	−0.0476	N/A[a]
$5s^2 \rightarrow p^2$	−0.4595	−0.5773	N/A[a]
$5s^2 \rightarrow d^2$ (incl. $4d$)	−0.0317	−0.0248	N/A[a]
$5s^2 \rightarrow f^2$	−0.0140	−0.0118	N/A[a]
$5s^2 \rightarrow g^2$	−0.0028	−0.0026	N/A[a]
$5s^2 \rightarrow pf+sd$	''0''	''0''	N/A[a]
$5s \rightarrow s$	−0.0342	−0.0314	0
$5s \rightarrow d$ (incl. $4d$)	−0.0143	−0.0142	−0.0100
$5s \rightarrow g$	−0.0172	−0.0172	−0.0028
$4d5s \rightarrow p^2$	−0.3446	−0.3461	−0.1354
$4d5s \rightarrow d^2$	−0.0085	−0.0085	−0.0049
$4d5s \rightarrow f^2$	−0.0165	−0.0165	−0.0098
$4d5s \rightarrow g^2$	−0.0052	−0.0051	−0.0018
$4d5s \rightarrow sd$	−0.2809	−0.2841	−0.1541
$4d5s \rightarrow pf$	−0.7799	−0.7755	−0.5420
$4d5s \rightarrow dg$	−0.0673	−0.0675	−0.0408
$4d5s \rightarrow fh$	−0.0205	−0.0207	−0.0137
$4d \rightarrow s$ (incl. $5s$)	−0.0173	−0.0172	−0.0131
$4d \rightarrow d$	−0.0682	−0.0682	−0.0469
$4d \rightarrow g$	−0.0922	−0.0922	−0.0990
$4p5s \rightarrow sp$	−0.0462	−0.0454	−0.0290
$4p5s \rightarrow pd$ (incl. $4d$)	−0.1706	−0.1678	−0.1446
$4p5s \rightarrow df$ (incl. $4d$)	−0.0493	−0.0493	−0.0319
$4p5s \rightarrow fg$	−0.0074	−0.0074	−0.0068
$4s5s \rightarrow s^2$	NC[b]	NC[b]	−0.0004
$4s5s \rightarrow p^2$	NC[b]	NC[b]	−0.0015
$4s5s \rightarrow d^2$ (incl. $4d$)	NC[b]	NC[b]	−0.0045
$4d5s^2 \rightarrow p^2d+pdf+pfg+sp^2+spf+s^2d+p^2g$	''0''	''0''	N/A[a]
$4p5s^2 \rightarrow pd^2+p^3+pf^2+spd+pdg$	''0''	''0''	N/A[a]
$4d^2 5s^2 \rightarrow p^2f^2+p^4+p^3f+p^2sd$	NC[b]	''0''	N/A[a]
$4p \rightarrow p+f$[c]	−1.7616		−1.7807
Breit	+0.0007		0

[a]N/A = not applicable to this state.
[b]NC = not calculated.
[c]Obtained via separate calculation (DF+$4p \rightarrow p+f$).

the experiments is obtained by using the first Stokes beam of Raman converted 8 ns laser light pulses from a Nd:YAG pumped dye-laser, operating at a 10 Hz repetition rate. The Raman conversion is obtained by focusing the dye laser light into a 120 cm long Raman cell filled with H_2 gas at 22(1) bar, producing a Stokes shift of 4155.197(20) cm^{-1} [21]. The anti-Stokes and pump laser beams are eliminated from the recollimated laser beam with dichroic mirrors and silicon semiconductor plates, or with optical glass filters, arranged at Brewster's angle and paired in order to compensate for beam walking as the laser frequency is tuned. The first Stokes laser light is allowed to pass through a vacuum viewport and interact with the negative ion beam in the UHV chamber. After having passed through a second viewport, the light is finally detected by a pulse-energy meter. Average pulse energies of 3.3–3.6 mJ are obtained in the UHV chamber. Since the photons of the weak ($\leq$0.5 mJ per pulse) second Stokes component are not sufficiently energetic to detach the negative ions of ruthenium, even from an excited state, no effort was made to filter that component from the beam.

A threshold energy is extracted by fitting a Wigner threshold law [22] to the collected data. For a photon energy ε and threshold energy ε_0, the Wigner threshold law states that the cross section for detachment vanishes for $\varepsilon \leq \varepsilon_0$, and is proportional to $(\varepsilon-\varepsilon_0)^{\ell+1/2}$ for $\varepsilon > \varepsilon_0$, where ℓ is the angular momentum of the detached electron. Therefore, since the electron is detached into a *p*-wave continuum in the case of Ru^-, we expect the cross section to have a $\frac{3}{2}$ power-law dependence on photon energy near the threshold.

IV. THEORETICAL RESULTS

RCI calculations begin by making single and pair excitations from the outermost *s* electrons; these pair excitations

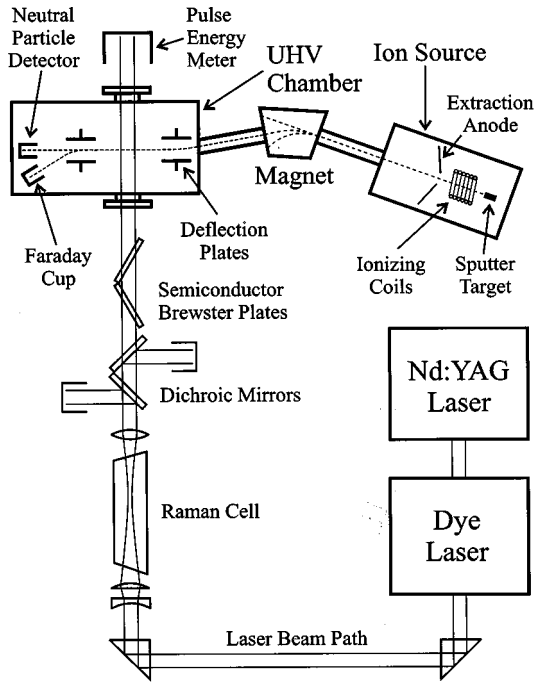

FIG. 1. Schematic illustrating the experimental apparatus (see accompanying text for details).

are present only in the negative ion. Energy contributions, determined by use of second-order perturbation theory [16], are shown in Table I for the $2J=9$ state of Ru^-. The most important of these valence correlations are $s^2 \rightarrow p^2$, $s \rightarrow s$, and $s^2 \rightarrow s^2$. We carefully monitor these contributions as we excite (open) from the core, and when we observe significant changes, introduce triple and quadruple excitations, which tend to partially compensate for these losses. Valence excitations seem (see Table I) to be adequately described by $l=0,4$ and by one radial function per l, except for the p symmetry, which uses two. The first p ''virtual'' is generated from a MCDF $5s^2+5p^2$ calculation.

The next step is to include the pair excitations $ds \rightarrow$ and single excitations from the d shell. These are major contributors to the Ru EA (the DF contributions are negative in fact), with the $ds \rightarrow sd+p^2+pf$ being the largest. As Table I shows, here it is necessary to include symmetries up to $l=5$. Introduction of these excitations decreases the valence contributions, particularly $s^2 \rightarrow p^2$, by as much as 100 meV. This number is obtained by comparing to a calculation where only excitations from $5s^2$ are allowed (not shown). This is partly because we have treated d^7s^2 and d^7p^2 unequally; we have included $ds \rightarrow$ in the former, but not dp excitations in the latter. When these are introduced (and they are triple excitations with respect to d^7s^2; the specific triples included are listed in Table I by symmetry type), about 1/3 of the energy lost is restored. Coefficients of these triples can be as large as 0.01 in magnitude. Both ds and dp excitations generated manifolds that are so complicated (number of parents, determinants) that the REDUCE methodology [13,14] is used to introduce them.

A nearly complete restoration, as compared to a calculation where only excitations from $5s^2$ are allowed (not shown), of the $5s^2 \rightarrow p^2$ valence correlation energy is achieved with the inclusion of the quadruple excitations $4d^25s^2 \rightarrow p^2f^2+p^4+p^3f+p^2sd$ using the newly modified REDUCE program [13]. Of these, the first is most important. The restoration can be most clearly seen by comparing the two Ru^- columns in Table I (without and with these quadruples). These differ by 98 meV, so the net effect on the binding energy for $2J=9$ is to increase it by 98 meV.

We note that no d^2 excitations are included here. We exclude them, because we believe their large contributions to the total energy make almost no contribution to the Ru EA. This seems confirmed by our DF + $\epsilon(5d^2)$ calculations on Os-Os^- [15]. Furthermore, if they were introduced they would have to be treated in a very balanced way (equivalent basis sets) for atom and ion, and they would have a significant impact on the valence correlations, necessitating the introduction of further (partially) compensating triple and quadruple excitations.

The next computation step is to include ps excitations. From Table I, it is seen these contribute 61 meV to the EA of Ru. Opening this shell also impacts the valence excitations, which is partially compensated for by the inclusion of pp' excitations from d^7p^2. In the process of opening this subshell, it was noted that there was a decrease in the important $ds \rightarrow pf$ contributions (there is a strong $d^2 \rightarrow pf$ interaction between the two, as expected [23]). It is important to note, however, that this change (total energy) had almost zero impact on the EA.

We also included the effect of $4p \rightarrow p+f$ excitations, by doing separate calculations (DF+$4p \rightarrow p+f$) so as to avoid the need for compensating triple excitations. The net effect is to lower the $2J=9$ binding energy by 19.1 meV.

For Ru $2J=10$, we also opened the $4s$ subshell. Since the contribution to the total energy is so small (6.4 meV), it has not been included in any of the Ru EAs. To simplify calculations for the $2J=7,5,3$ Ru^- states, we argue as in Sn^- [12] that there is much correlation in common with the $2J=9$ state. There is a ''first-order'' theoretical basis for this [24], which applies if (among other conditions) the radial functions for the states do not vary much, and at least one of the two subshells being excited is initially closed. Greater cancellation also ensues because all ion states are associated (mainly) with the same $d^7\,{}^4F$ configuration. In this case, we specifically have not opened the p subshell for the $2J=7,5,3$ states, locating them instead with respect to the $2J=9$ state (using a wave function with the p subshell closed).

The binding energies for all states are reported in Table II. Those for $2J=9$ may be extracted from Table I using the formula BE = DF + CA−CI−Breit, where CA (CI) is the correlation energy for the atom (ion). It can be seen that the ion is unbound at the DF level and the Breit contribution is small. Because the binding energies are quite large, we looked at the first excited negative ion state for all J's, but none of these appear bound (all had d^7s^2 configurations). We also did a MCDF ($5s^2+5p^2$) calculation for $2J=1$, and found the energy to be 1.301 eV above the MCDF energy of the Ru^- $2J=3$ state, suggesting that $2J=1$ is not bound.

Table II also includes results for magnetic dipole (A) and electric quadrupole/quadrupole moment (B/Q) constants. Nuclear constants are taken from Fuller and Cohen [25] and Raghavan [26]. For Ru I, very accurate experimental results are available [27] for A and B/Q. Our results are in good agreement with these, though the accuracy could be im-

TABLE II. Binding energies (BE), hyperfine structure constants (A,B), and magnetic dipole decay rates (A).

State	BE (eV)			HFS[b] A (MHz)			B/Q (MHz/b)			$M1$ (s^{-1})[c]
	DF	corr	Total[a]	DF	RCI	Expt.	DF	RCI	Expt.	A[d]
$Ru^- 4d^7 5s^2$										
$2J=9$	−0.3167	1.3866	1.076	−90	−113		338	302		N/A[e]
			1.05(15)[f]							
			1.04638(25)[g]							
$2J=7$	−0.4936	1.3833	0.905	−97	−97		243	220		0.213
			0.8653(10)[g]							
$2J=5$	−0.6080	1.3832	0.795	−117	−111		180	162		0.0229
$2J=3$	−0.6802	1.3819	0.725	−192	−165		168	151		0.00741
Ru $4d^7 5s$										
$2J=10$	N/A[e]	N/A[e]	N/A[e]	1043	1052	948[h]	529	448	459[h]	N/A[e]

[a]DF + corr. + magnetic Breit.

[b]For Ru/Ru^-, $\mu=-0.69$, $I=5/2$, $Q=0.457$ barns; μ and I from Fuller and Cohen [25], and Q from Raghavan [26].

[c]In accordance with magnetic dipole selection rules $(dJ=0,\pm1)$, decay from the J level occurs only to the $J+1$ level.

[d]RCI values; DF values differ ~1%.

[e]N/A = not applicable to this state.

[f]Semiempirical (extrapolated) value from Feigerle *et al.* [3].

[g]Experimental result from this work.

[h]Experimental values [27] for HFS are given to more significant figures.

proved by including core excitations such as $4s\rightarrow s+d$ and $4p\rightarrow p+f$, as we do in more thorough HFS studies [16]. Finally, Table II contains RCI magnetic dipole decay rates for the ion states; these differ little (1%) from the DF values.

V. EXPERIMENTAL RESULTS

The energy level structure of Ru^- is illustrated in Fig. 2. A portion of the data collected from a series of coarse scans, covering photon energies of 7275–9930 cm^{-1}, is shown in Fig. 3. The higher-energy threshold seen here is identified with the $^4F_{9/2}\rightarrow{}^5F_5$ detachment channel, since this channel is expected to be the strongest. Using a ''cool'' cathode configuration, in order to suppress the background from lower

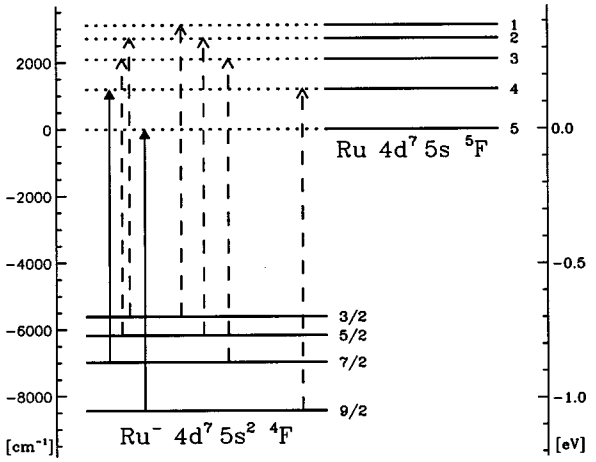

FIG. 2. Energy level diagram of Ru^- and the Ru ground state. The arrows, indicating the allowed detachment thresholds, are spaced proportionally to the threshold energies and ordered by increasing energy from left to right. The solid arrows indicate the thresholds observed in the present study; the other thresholds are dashed.

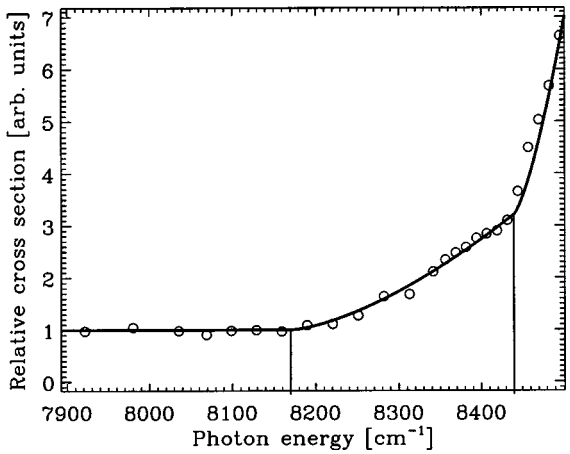

FIG. 3. A portion of the region covered by the series of coarse scans discussed in the text. The higher-energy threshold seen here is the $^4F_{9/2}\rightarrow{}^5F_5$ detachment threshold of Ru^- (see Fig. 4) and the lower-energy threshold corresponds to the $^4F_{7/2}\rightarrow{}^5F_4$ detachment threshold (see Fig. 5). The solid curve was calculated assuming the measured threshold positions (indicated by vertical lines), determined from high-resolution scans. Each data point represents the sum of the signal from 1000 laser pulses. Note that this data was collected with a ''hot'' cathode, so while the relative cross-section scale in this figure does match that of Fig. 5, it does not match that of Fig. 4.

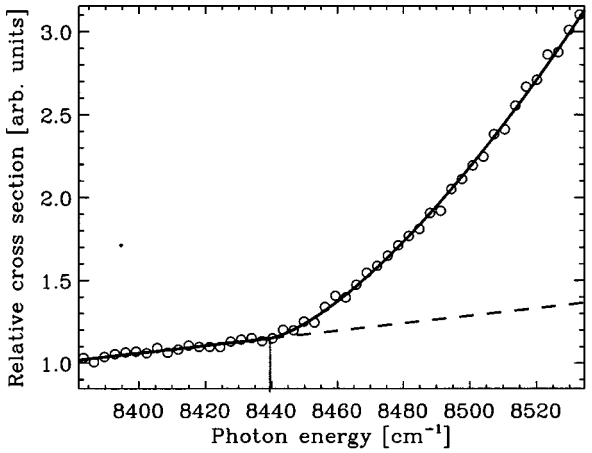

FIG. 4. The $^4F_{9/2}\rightarrow{}^5F_5$ detachment threshold of Ru^-. The solid curve represents the fitted Wigner *p* wave, including a sloped background, with the best-fit threshold position indicated by the vertical line. The below-threshold signal (extrapolated with the broken line) is largely due to detachment from the excited states of Ru^- (see Fig. 3). Each data point represents the signal collected from 2000 laser pulses. The data for this plot were collected with a ''cool'' source in order to minimize the background signal due to excited-state population.

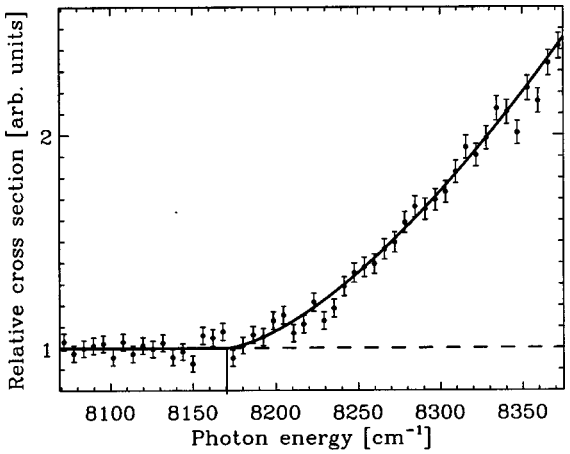

FIG. 5. The $^4F_{7/2}\rightarrow{}^5F_4$ detachment threshold of Ru^-. The solid curve is the Wigner *p*-wave fit, with the vertical line indicating the best-fit threshold position. The background signal observed here (extrapolated with the dashed line) remains constant over a large range (see text for details). Individual data points represent the signal obtained from 2000 laser pulses. Error bars are one standard deviation, estimated on the basis of counting statistics. To increase the threshold strength, a ''hot'' ion source was used here.

thresholds (see discussion below), an ≈ 150 cm^{-1} range is selected and repeatedly scanned at a much higher resolution. Figure 4 presents the result of these scans. As can be seen by the fitted solid curve, the expected $\frac{3}{2}$ power-law behavior agrees well with the data, and yields a best-fit threshold energy of 8439.6(20) cm^{-1} (all quoted uncertainties are to one standard deviation and include the systematic errors associated with this apparatus of <0.1 cm^{-1} [21]). Therefore the binding energy of the $^4F_{9/2}$ level, and hence the EA of Ru, is 8439.6(20) cm^{-1} [1.046 38(25) eV, using 8065.5410(24) cm^{-1} eV^{-1} [28]].

Table III lists relative threshold strengths for a ''cool'' (650 K) and a ''hot'' (1300 K) ion source, assuming a thermal distribution and *L*-*S* coupling [5]. As can be seen from the table, only two other thresholds have a sufficiently high fractional intensity to likely be observed: the $^4F_{7/2}\rightarrow{}^5F_4$ and $^4F_{9/2}\rightarrow{}^5F_4$ detachment thresholds. The latter threshold would be difficult to observe because of the large background signal that would be present from the other seven lower-energy detachment channels. Furthermore, no additional information would be obtained about the negative ion, since the $^4F_{9/2}$ level can be accurately positioned from the observed $^4F_{9/2}\rightarrow{}^5F_5$ threshold (Fig. 4). Therefore, running the ion source ''hot,'' a selected region of ≈ 300 cm^{-1} around the lower energy threshold of Fig. 3, is repeatedly scanned at a high resolution. The result of this set of scans is presented in Fig. 5, where the solid curve represents the best-fit Wigner law with a threshold value of 8170(8) cm^{-1}. Since the signal below this threshold appears to remain constant over the entire range of photon energies of 7275–8150 cm^{-1}, it is improbable that this signal is a result of detachment from a higher-lying excited state of Ru^-, but rather is likely due to a small amount of mass-coincident or nearly mass-coincident impurity molecules such as hydrides. Considering the predicted relative threshold strengths and the ranges scanned, we must assign this second threshold to detachment from the negative ion $^4F_{7/2}$ level to the neutral atom $^5F_4$ level (the leftmost arrow appearing in Fig. 2). By subtracting the $^5F_5$-$^5F_4$ neutral atom splitting of 1190.64 cm^{-1} [29] from the measured threshold energy, we obtain a binding energy for the $^4F_{7/2}$ level of 6979(8) cm^{-1} [0.8653(10) eV]. As a further check, a scan of the $^4F_{9/2}\rightarrow{}^5F_5$ threshold is repeated immediately following the high-resolution $^4F_{7/2}\rightarrow{}^5F_4$ scans. Comparing the amplitudes of the Wigner fits to these two data sets yields an experimental relative strength for the $^4F_{7/2}\rightarrow{}^5F_4$ detachment, with a ''hot'' ion source, of 12(1) percent, in reasonable agreement with the expected threshold intensity given in Table III.

TABLE III. Calculated intensities of Ru^- thresholds.

Threshold[a]	Relative intensity [b] $T=650$ K	$T=1300$ K	$T=\infty$ [c]
$^4F_{7/2}\rightarrow{}^5F_4$	2.7	13.6	68.2
$^4F_{5/2}\rightarrow{}^5F_3$	0.3	3.3	40.9
$^4F_{3/2}\rightarrow{}^5F_2$	<0.1	0.8	18.2
$^4F_{9/2}\rightarrow{}^5F_5$	100.0	100.0	100.0
$^4F_{3/2}\rightarrow{}^5F_1$	0.1	1.2	27.3
$^4F_{5/2}\rightarrow{}^5F_2$	0.2	2.2	27.3
$^4F_{7/2}\rightarrow{}^5F_3$	0.9	4.5	22.7
$^4F_{9/2}\rightarrow{}^5F_4$	13.6	13.6	13.6

[a]Thresholds are ordered from low to high energies.

[b]Relative intensities are given in percent of the strongest detachment channel.

[c]In the $T=\infty$ case, the population is distributed according to *L*-*S* coupling statistics only, and therefore yields the largest relative intensities that can be obtained from a ''thermal'' ion source.

VI. CONCLUSION AND SUMMARY

In summary, the binding energies of the ^4F $2J=9$ and $2J=7$ levels of Ru^- were successfully measured with infra-

red LPT experiments. The binding energies of the $2J=5$ and $2J=3$ levels were not measured, primarily because of the very low relative intensities of the associated detachment thresholds. It may be possible to increase the detachment signals from these levels by using an alternate ''nonthermal'' ion production mechanism (such as charge exchange in a metal vapor cell) to increase excited state populations. In addition, a channel-sensitive LPT approach, similar to that used by Dellwo *et al.* on Li^- [30], might allow measurements of the higher-energy thresholds that are difficult to observe due to a large background signal from the lower-lying detachment channels.

The theoretical results for the $2J=9$ and $2J=7$ binding energies are in excellent agreement with experiment. We have identified (and calculated) the important role that a few quadruple excitations have on the Ru EA. The treatment has been sufficiently automated to permit their inclusion in a variety of problems. As might be expected, due to the similarity of correlation effects, the $2J=9\rightarrow 2J=7$ splitting is determined more accurately (~ 10 meV uncertainty) than the absolute value of the $2J=9$ binding energy (~ 30 meV uncertainty).

ACKNOWLEDGMENTS

Support from the National Science Foundation under Grant 96-05213 for the theoretical part of this work is gratefully acknowledged. We are also thankful to the National Research Council of Canada (NSERC) for providing the funding for the experimental work.

[1] T. Andersen, H. H. Andersen, P. Balling, P. Kristensen, and V. V. Petrunin, J. Phys. B **30**, 3317 (1997).
[2] H. Hotop and W. C. Lineberger, J. Phys. Chem. Ref. Data **14**, 731 (1985).
[3] C. S. Feigerle, R. R. Corderman, S. V. Bobashev, and W. C. Lineberger, J. Chem. Phys. **74**, 1580 (1981).
[4] R. C. Bilodeau, M. Scheer, and H. K. Haugen, J. Phys. B **31**, 3885 (1998).
[5] M. Scheer, C. A. Brodie, R. C. Bilodeau, and H. K. Haugen, Phys. Rev. A **58**, 2051 (1998).
[6] See, e.g., W. P. Wijesundera, Phys. Rev. A **55**, 1785 (1997).
[7] E. N. Avgoustoglou and D. R. Beck, Phys. Rev. A **55**, 4143 (1997).
[8] See, e.g., E. Eliav, Y. Ishikawa, P. Pyykko, and U. Kaldor, Phys. Rev. A **56**, 4532 (1997).
[9] See, e.g., V. A. Dzuba and G. F. Gribakin, Phys. Rev. A **55**, 2443 (1997).
[10] J. P. Desclaux, Comput. Phys. Commun. **9**, 31 (1975).
[11] D. R. Beck, program RCI (unpublished).
[12] S. M. O'Malley and D. R. Beck, Phys. Rev. A **57**, 1743 (1998).
[13] D. R. Beck, program REDUCE (unpublished).
[14] D. R. Beck and D. Datta, Phys. Rev. A **48**, 182 (1993).
[15] P. L. Norquist and D. R. Beck (unpublished).
[16] S. M. O'Malley and D. R. Beck, Phys. Rev. A **54**, 3894 (1996).
[17] I. Lindgren and A. Rosen, Case Stud. At. Phys. **4**, 93 (1974).
[18] I. P. Grant, J. Phys. B **7**, 1458 (1974).
[19] D. R. Beck and Z. Cai, Phys. Rev. A **41**, 301 (1990).
[20] H. F. King *et al.*, J. Chem. Phys. **47**, 1936 (1967).
[21] M. Scheer, R. C. Bilodeau, C. A. Brodie, and H. K. Haugen, Phys. Rev. A **58**, 2844 (1998).
[22] E. P. Wigner, Phys. Rev. **73**, 1002 (1948).
[23] D. R. Beck and C. A. Nicolaides, Phys. Rev. A **26**, 857 (1982).
[24] D. Datta and D. R. Beck, Phys. Rev. A **47**, 5198 (1993).
[25] G. H. Fuller and V. W. Cohen, At. Data Nucl. Data Tables **5**, 433 (1969).
[26] P. Raghavan, At. Data Nucl. Data Tables **42**, 189 (1989).
[27] S. Buttgenbach, *Hyperfine Structure in 4d- and 5d- Shell Atoms* (Springer-Verlag, New York, 1982).
[28] E. R. Cohen and B. N. Taylor, Rev. Mod. Phys. **59**, 1121 (1987).
[29] C. E. Moore, *Atomic Energy Levels* (U.S. GPO, Washington, D.C., 1971), NSRDS-NBS 35.
[30] J. Dellwo, Y. Liu, D. J. Pegg, and G. D. Alton, Phys. Rev. A **45**, 1544 (1992).